# Nonresonant beat-wave excitation of relativistic plasma waves with constant phase velocity for charged-particle acceleration

C. V. Filip,[1,*] R. Narang,[1] S. Ya. Tochitsky,[1] C. E. Clayton,[1] P. Musumeci,[2] R. B. Yoder,[2] K. A. Marsh,[1] J. B. Rosenzweig,[2] C. Pellegrini,[2] and C. Joshi[1]

[1]*Neptune Laboratory, Department of Electrical Engineering, UCLA, 405 Hilgard Avenue, Los Angeles, California 90095, USA*

[2]*Department of Physics, UCLA, 405 Hilgard Avenue, Los Angeles, California 90095, USA*

(Received 26 June 2003; published 17 February 2004)

The nonresonant beat-wave excitation of relativistic plasma waves is studied in two-dimensional simulations and experiments. It is shown through simulations that, as opposed to the resonant case, the accelerating electric fields associated with the nonresonant plasmons are always in phase with the beat-pattern of the laser pulse. The excitation of such nonresonant relativistic plasma waves is shown to be possible for plasma densities as high as 14 times the resonant density. The density fluctuations and the fields associated with these waves have significant magnitudes, facts confirmed experimentally using collinear Thomson scattering and electron injection, respectively. The applicability of these results towards eventual phase-locked acceleration of prebunched and externally injected electrons is discussed.

DOI: 10.1103/PhysRevE.69.026404 PACS number(s): 52.35.Mw, 41.75.Jv, 52.70.Kz, 52.38.Kd

## I. INTRODUCTION

Electron plasma waves that propagate with a phase velocity close to $c$ have been proposed as high-gradient accelerating structures for charged particles [1]. Such relativistic plasma waves (RPW's) have been excited using laser and charged particle beams [2]. An intense, two-frequency laser pulse ($\omega_1$ and $\omega_2$) propagating through a plasma can excite such a RPW in, what is known as, a plasma beat-wave accelerator (PBWA) [3]. The excitation process is most efficient at the resonant density $n_{\mathrm{res}}$, when the beat frequency $\Delta\omega=\omega_1-\omega_2$, is equal to the plasma frequency $\omega_p$. Furthermore, electrons have been externally injected in these resonantly excited RPW's and shown to gain energy [4,5]. However, in these experiments, no attempt was made to phase lock the electrons with the RPW and consequently, the accelerated electrons had a broad and continuous energy spectrum.

For many applications of high-energy particles one needs a nearly monoenergetic beam. To obtain monoenergetic acceleration, the externally injected relativistic electrons are tightly (less a tenth of a plasma wavelength) prebunched with the same periodicity as the laser beat pattern that is also used to excite the RPW's [6,7]. In the ideal case, it is then possible to maintain the phase synchronism between the injected electrons and the accelerating structure. Successful acceleration of phase-locked electrons, in which the RPW has typically a submillimeter wavelength, will depend on four factors: ability to prebunch, ability to load the prebunched electrons within the acceptance of the RPW structure, control of the experimental time ($<100$ fs) and space ($<50\ \mu$m) jitter, and control of the phase jitter introduced by the RPW itself. This last factor can be a serious problem in resonant excitation of RPW's using the laser beat-wave technique. Transverse and longitudinal plasma inhomogeneities, relativistic saturation of the plasma wave near resonant densities, small deviations from the exact resonance condition in an otherwise uniform plasma, and fluctuations in the laser intensity and rise time, can all dephase the beat wave driver and therefore the prebunched electrons with respect to the RPW. We have therefore explored a possible solution to this issue in which the RPW is nonresonantly excited at plasma densities much greater than the resonant density $n\gg n_{\mathrm{res}}$.

Conceptually, it is well known that a harmonic oscillator driven far away from its resonance remains synchronous with the driving force albeit with a smaller amplitude of oscillation than that at resonance. Using two-dimensional (2D) particle-in-cell (PIC) computer simulations we find that, as opposed to the resonant case, the nonresonantly excited plasmons are similarly always in phase with the beat pattern of the laser pulse. Although the normalized amplitude of the oscillation is smaller, the longitudinal electric field of such a wave can still be substantial if the plasma density is much higher than the resonant density. Experimentally, we have shown that such high accelerating fields can be excited in plasmas with densities up to $14n_{\mathrm{res}}$. We have diagnosed these fields through collinear Thomson scattering of a probe laser beam and by measuring the energy gained by externally injected relativistic electrons. These results indicate that nonresonantly excited RPW's may be suitable for phase-locked injection in the second generation PBWA experiments, where the goal is to demonstrate a high-gradient monoenergetic electron acceleration [2].

## II. SIMULATIONS

### A. Resonant excitation

The excitation process of a RPW when $\Delta\omega=\omega_p$ was investigated by Rosenbluth and Liu [8]. They showed that the amplitude of the plasma wave $\varepsilon=\delta n/n$ is limited to $\varepsilon<1$ by an amplitude dependent phase shift, which saturates the plasma wave. Here, $\delta n/n$ is the normalized density pertur-

*Author to whom correspondence should be addressed; electronic address: cfilip@ucla.edu

 ©2004 The American Physical Society

bation associated with the plasma wave. This study was followed by Tang *et al.* [9], who proposed to compensate for this ''relativistic'' saturation by employing a density detuning. Other analytical and numerical 1D studies have also investigated the critical issue of RPW dephasing with [10] and without density inhomogeneities [11,12]. Here we analyze the electron-plasmon interaction in space and time *during* the acceleration process in 2D, using a PIC code where no analytical solutions exist.

We use the code TURBOWAVE that includes ionization of gas and mobile ions [13] to model the growth and saturation of the beat wave-driven RPW and in particular to follow the phase relationship between the plasmon and the driver. We first illustrate the dephasing induced by plasma density inhomogeneities introduced by the ponderomotive force of the laser pulse. This is done by choosing the ratio of the plasma wavelength to the spot size of the laser beam to be 6. For a $CO_2$ laser, used in the experiments described later in the paper, this corresponds to a spot size $w_0$ of 50 $\mu$m. The 50-ps (FWHM), two-frequency pulse with $\omega_1, \omega_2/\omega_p \sim 30$ and $a_1 = a_2 = 0.3$ propagates in hydrogen ($a_1$ and $a_2$ are the normalized vector potentials corresponding to each frequency). The temporal shape of the laser pulse is given by a fifth order polynomial function. The transverse profile of the focussed beam is approximately Gaussian [13]. The beat period is $\sim 1.1$ ps. The gas is tunnelionized and plasma is formed with a density initially above resonance $n = 1.3 n_{\mathrm{res}}$. The plasma density decreases in the focal region with a maximum $dn/dt = -0.8\% n/\mathrm{ps}$ due to the transverse ponderomotive force of the laser pulse which expels the plasma electrons. Therefore, $n$ is a function of the longitudinal ($x$) and transverse ($y$) positions and time, $n = n(x,y,t)$. To illustrate how the variations in the plasma density affect the saturation process of the RPW, Fig. 1(a) shows a snapshot of the longitudinal electric field $E_x$ associated with the RPW. The area that was selected to be shown in Fig. 1(a) is part of a larger box ($4.8 \times 1.2$ mm$^2$) used in this simulation. Figure 1(b) shows a horizontal lineout through the center of Fig. 1(a), which is also the axis of symmetry of the laser beam. The laser pulse propagates from left to right. In the absence of the plasma, the position of the ''vacuum'' focus of the laser beam would be close to the center of the 2D simulation box as indicated by the black arrow in Fig. 1(a).

Following ionization, the plasma density slowly begins to decrease in the focal region as a result of the ponderomotive blowout. The RPW grows faster here than upstream and downstream of the best focus, especially when the plasma density approaches $n_{\mathrm{res}}$. The phase velocity of the wave begins to drop below $c$, reaching a minimum when $\varepsilon$ is close to its maximum value. In other words, in the focal region, the wave is slowing down. This effect is visible in Figs. 1(a) and 1(b) around $x = 1$ mm, where the wave fronts of the plasma wave are ''squeezed'' compared to the region downstream of the focus. The snapshot is taken at $t = 53$ ps after the front of laser pulse reached the center of the simulation box. To better illustrate this effect and to quantify the evolution of the phase velocity $v_{\mathrm{ph}}$, a crest of the RPW which enters the simulation box on axis at $x = 0$ mm and $t = 47.5$ ps is followed in space and time. The dots in Fig. 2(a) show the dependence of the

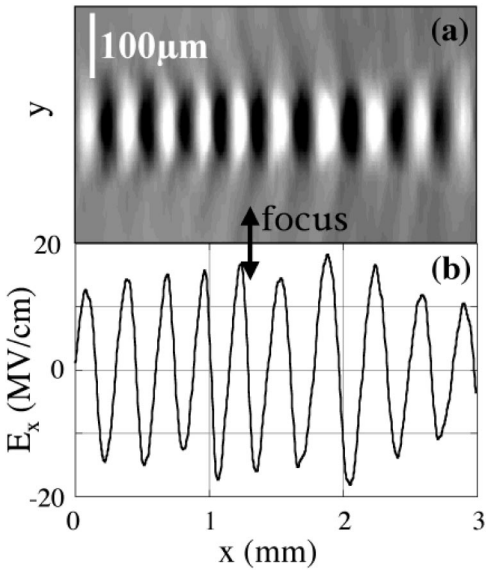


FIG. 1. (a) Snapshot of the longitudinal electric field $E_x$ associated with the RPW at 53 ps after the front of the pump pulse, moving from left to right, reached the center of the simulation box; $y$ and $x$ are the transverse and longitudinal directions, respectively. The initial plasma density is $n = 1.3 n_{\mathrm{res}}$. (b) Horizontal lineout through (a). The black arrow indicates the location of the vacuum focus.

position of the crest versus time $x = x(t)$. The solid straight line is the speed-of-light trajectory that is followed by the beat pattern of the laser pulse which moves with a nearly constant group velocity $v_g \sim 0.9994c$ during this simulation.

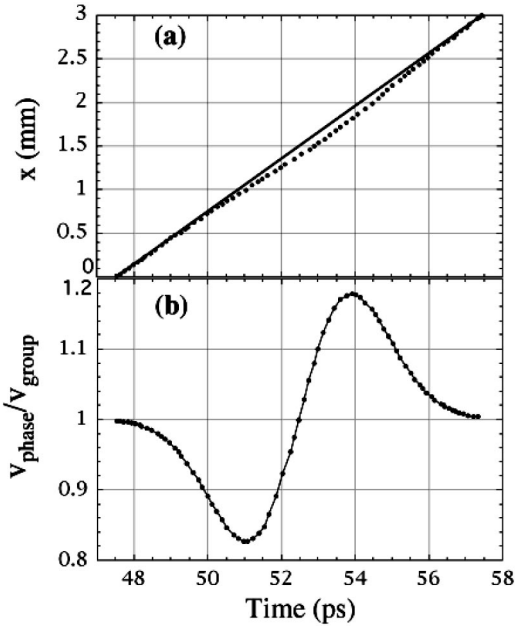


FIG. 2. (a) Horizontal position $x$ of a crest of the plasma wave that enters the simulation box at $x = 0$ and $t = 47.5$ ps versus time (dots) and the speed-of-light trajectory (solid line). The initial plasma density is $n = 1.3 n_{\mathrm{res}}$. (b) The ratio of the instantaneous phase velocity of the plasma wave to the group velocity of the laser pulse versus time, obtained from (a).

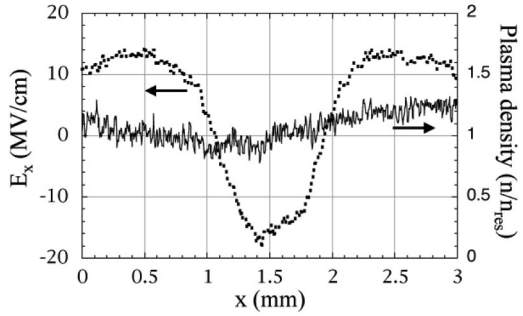


FIG. 3. Longitudinal electric field $E_x$ seen by a ''virtual'' relativistic electron injected on-axis at $x=0$ and $t\cong 47.5$ ps at the speed of light versus its position $x$ in the plasma (left axis, dotted line) for $n=1.3n_{\mathrm{res}}$. Axial profile of the plasma density, normalized to $n_{\mathrm{res}}$, at the injection time (right axis, solid line).

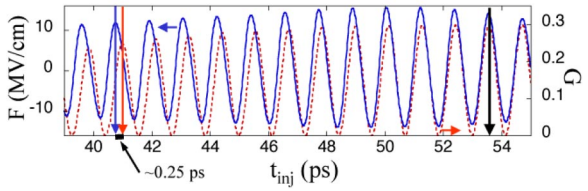


FIG. 4. The solid curve (left axis) shows the trajectory-averaged electric field $F$ seen by a relativistic electron injected on axis (at $x=0$) versus the injection time $F=F(t_{\mathrm{inj}})$. The dotted curve (right axis) shows the trajectory-averaged normalized laser intensity $G$ that the electron is riding along with in the plasma, versus the injection time $G=G(t_{\mathrm{inj}})$. The initial plasma density is $n=1.3n_{\mathrm{res}}$. The separation (phase) between the maxima of $F$ and $G$ is changing from $\sim 0.25$ ps, see the vertical arrows at $t_{\mathrm{inj}}\cong 40$ ps, to approximately 0 ps (see the arrow at $t_{\mathrm{inj}}\cong 54$ ps).

The departure of the dots from the straight line illustrates the dephasing of the RPW with respect to the laser pulse. The instantaneous phase velocity $v_{\mathrm{ph}}$ of the RPW is determined by taking the derivative of a curve that best fits the dots in Fig. 2(a). The ratio $v_{\mathrm{ph}}/v_g$ is shown in Fig. 2(b). The RPW slows down to $\sim 0.82c$ in the region upstream of focus and ''speeds up'' to $\sim 1.18c$ downstream of focus. This behavior of the phase velocity of the RPW is due mainly to the longitudinal variations in the plasma density caused by the ponderomotive force of the laser pulse and not to relativistic detuning.

The continuous dephasing of the RPW can have a profound influence on a relativistic electron that is injected at $x=0$ at a particular phase, and initially moving synchronously with it. The maximum spatial separation $\Delta x$ accumulated between the electron and the RPW can be found from Fig. 2(a) to be $\Delta x\cong 135\ \mu$m, which is close to half of a plasma wavelength. Therefore, it is possible for the electron to interact with both positive and negative fields. The electric field $E_x$ seen by a ''virtual'' relativistic electron initially injected on axis at $x=0$ and $t_{\mathrm{inj}}\cong 47.5$ ps is shown in Fig. 3 (dotted line). Figure 3 also shows the longitudinal plasma density profile at the time of the injection (solid line). The electron feels a positive electric field upstream and downstream of the focus, but in the focal region it is significantly decelerated as a result of the rapid dephasing represented in Fig. 2. The electric field $E_x$ has a strong dependence not only on the position of the electron, but also on the injection time $t_{\mathrm{inj}}$. To find out what is the influence of the dephasing on the overall energy gain for an electron injected at an arbitrary $t_{\mathrm{inj}}$, we introduce two new quantities $F$ and $G$. The quantity $F$, calculated for each injection time, $F=F(t_{\mathrm{inj}})$, is the electric field averaged over a certain interaction length $L$, where the RPW's are driven. This quantity, multiplied by the interaction length, gives the overall energy gain achieved by the electron. In a similar way, $G$ represents the normalized laser intensity that an injected electron would ''ride'' along with in the plasma, averaged over the same $L$, for each injection time $G=G(t_{\mathrm{inj}})$. The interaction length $L$ that the average is performed over is taken to be 3 mm. These two ''trajectory-averaged'' quantities $F$ and $G$, are presented in Fig. 4 as a function of $t_{\mathrm{inj}}$ for a selected time interval that was specifically chosen to show a clear change in the relative phase between $F$ (solid curve) and $G$ (dotted curve). Over approximately 11 laser beat periods, from $t_{\mathrm{inj}}\cong 41$ ps to $t_{\mathrm{inj}}\cong 53$ ps, the separation between the maxima of the two quantities $F$ and $G$ changes from $\Delta t\cong 0.25$ ps, see vertical arrows on the left side of Fig. 4, to $\Delta t\cong 0$ ps (see vertical arrow on the right side of Fig. 4). Such a phase shift between $F$ and $G$ could force an externally injected electron phase locked with $G$ to ''miss'' the proper injection phase that maximizes $F$ by as much as 25% of a beat period. As a result, the electron would see a smaller overall accelerating field, as it is the case presented in Fig. 3, where the injected electron, instead of being accelerated with the maximum of $F\cong 15$ MV/cm, sees a much smaller trajectory-averaged accelerating gradient of $\sim 4$ MV/cm.

The decrease in the overall accelerating field is not the only negative aspect that results from the local dephasing of the RPW. This dephasing can also affect the acceleration of short, multiple bunches of injected electrons that are phase-locked to the beat pattern of the laser pulse. Each bunch will be accelerated by electric fields with different values because of the gradual dephasing between F and G from bunch to bunch, as it is shown in Fig. 4. This will result in a significant spread in the energy gained by these bunches. If one single bunch is to be injected at the proper phase that maximizes the overall accelerating field $F$, then it is possible to obtain a narrow spread in the energy gained by the electrons for as long as the parameters of the excitation process of the RPW are kept the same, shot after shot. 2D simulations with small changes (few percent) in the initial plasma density and/or the laser pulse rise time and intensity were performed. The results showed that the phase detuning between the driver ($G$) and the RPW ($F$) is highly sensitive of these parameters, especially the plasma density. In reality, it is difficult to obtain and maintain an uniform, long, high-density plasma shot after shot, due to phenomena such as the ponderomotive blowout, partial and multistage ionization, ionization-induced refraction, and density inhomogeneities. Therefore, in a resonant PBWA, the dephasing between the driver and the plasma wave cannot be easily controlled and it could adversely influence the reproducibility of the electron energy gain.

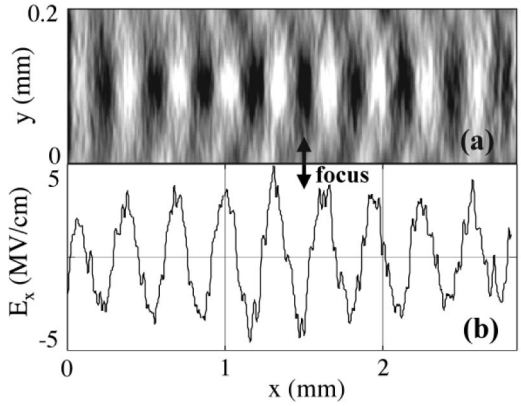


FIG. 5. (a) Snapshot of the longitudinal electric field $E_x$ associated with the RPW at 53 ps after the front of the pump pulse, moving from left to right, reached the center of the simulation box; $y$ and $x$ are the transverse and longitudinal directions, respectively. The initial plasma density is $n=7n_{\mathrm{res}}$. (b) Horizontal lineout through (a). The arrow indicates the location of the vacuum focus.

### B. Nonresonant excitation

Now let us consider the highly nonresonant excitation of the RPW's in a PBWA. As an example we show results of simulations that were carried out at a plasma density $n=7n_{\mathrm{res}}$. All other parameters are the same as the ones mentioned earlier. Forced plasma oscillations are excited by the two-frequency laser pulse. These oscillations represent a RPW that has a phase velocity $v_{\mathrm{ph}}$ equal to the local group velocity of the laser pulse in the plasma. Note that the higher density changes the effective relativistic Lorentz factor $\gamma_{\mathrm{ph}} \cong \omega_1/\omega_p$ associated with this RPW compared to that at the exact resonance. Even though the homogeneous response of the plasma might have triggered the onset of the Raman Forward instability, no relativistic waves with a frequency of $\omega_p$ were observed in the simulations. Figure 5(a) shows a typical snapshot of the longitudinal ($E_x$) field associated with the plasma wave. The wave vector of the plasma wave is $\Delta k$, where $\Delta k=k_1-k_2$ and $k_1$ and $k_2$ are the wave vectors of the pump pulse. The frequency of the plasma wave is again $\Delta\omega$ (from additional measurements performed in time, not shown). Other simulations were performed at different densities with similar results. No nonlinear saturation process has been observed. The $E_x$ field maintains the profile shown in Fig. 5(a) for as long as the pump pulse of an approximately constant amplitude is present in the plasma even though the ponderomotive blowout decreases the plasma density in the focal region by $\sim 20\%$. Figure 5(b) shows a lineout of the $E_x$ along the axis of the laser beam. Even though in this case the wave amplitude $\varepsilon=\delta n/n$ is small, $\varepsilon\sim 1.8\%$, the maximum local value of $E_x$ is quite high, $E_x=5$ MV/cm. This is, because, according to Poisson's equation, the electric field is a function of the perturbed density $\delta n$ and not $\varepsilon$.

As an example, in 1D, a 1% wave excited at $n=10n_{\mathrm{res}}$ has the same accelerating field as a 10% wave at resonance. The 1D result is not valid for a 2D (or a 3D) wave due to the transverse electric fields associated with $\delta n$. The exact relationship between $E_x$ and $\varepsilon$ can only be extracted from the simulation results. We have observed that tightly focussed laser beams drive higher (than 1D) amplitude waves off resonance. This can be seen in Fig. 6(a) which shows the maximum amplitude $\varepsilon_{\mathrm{max}}$ of the RPW's obtained from 1D and 2D ($w_0=50\ \mu$m) simulation results from the PIC code for a range of plasma densities from $0.5n_{\mathrm{res}}$ to $14n_{\mathrm{res}}$. The $\varepsilon_{\mathrm{max}}$ at resonance, shown in Fig. 6(a) for the 1D case, is approximately 75%, very close to the 78% value predicted by the 1D analytical model of Ref. [8]. The 2D simulations included the formation of the plasma by tunnel ionization of hydrogen and mobile ions. The reason why the 2D values of $\varepsilon_{\mathrm{max}}$ are higher than the 1D values is that, with tightly focussed beams, both the radial and axial oscillations can contribute to the density perturbation $\delta n$.

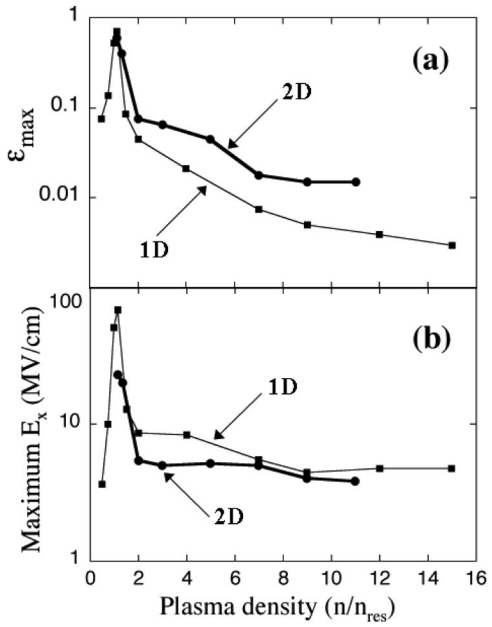


FIG. 6. (a) Maximum local amplitudes of the RPW's $\varepsilon_{\mathrm{max}}$ excited by a 50-ps pulse with normalized vector potentials of $a_1=a_2=0.3$, 1D (squares, thin line) and 2D ($w_0=50\ \mu$m, circles, thick line) versus the plasma density normalized to $n_{\mathrm{res}}$. (b) Maximum values of the longitudinal electric fields $E_x$ associated with the RPW's shown in (a).

The PIC simulations can also provide the maximum local value for the longitudinal electric field $E_x$ associated with the 1D and 2D RPW's whose amplitudes were presented in Fig. 6(a). These values are shown in Fig. 6(b) for the 1D case (squares), and for the 2D case (circles). Surprisingly, although the amplitude of the density perturbations in the 2D simulations are higher than the 1D simulations, the value of the maximum $E_x$ is the same or somewhat smaller. This is thought to be because of the significant radial component of the electric field associated to the RPW's produced by tightly focussed beams. The maximum $E_x$ for a wide range of plasma densities of $(2-11)n_{\mathrm{res}}$ is approximately constant at around 5 MV/cm, a value that is 4.6 times smaller than the peak value of $E_x$ of $\sim 23$ MV/cm at resonance. The advantage that the nonresonantly excited fields have compared to the resonantly excited fields is that the former are insensitive to the exact value of the plasma density (in space and time)

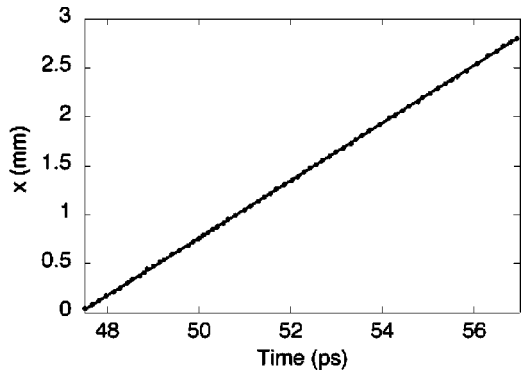


FIG. 7. Horizontal position $x$ of a crest of the plasma wave that enters the simulation box at $x=0$ and $t=47.5$ ps versus time (dots) and the speed-of-light trajectory (solid line). The initial plasma density is $n=7n_{\mathrm{res}}$.

and, more important, as we shall see, they are phase locked with respect to the beat pattern of the laser pulse. The phase velocity of the RPW excited at $n=7n_{\mathrm{res}}$ can be determined using the same technique as was used in Fig. 2, i.e., by following a crest of the $E_x$ associated with the wave in space and time. Figure 7 shows the position $x$ of a given crest on axis versus time. The round dots mark the moments when the position of the crest was recorded and the solid line represents the speed-of-light trajectory. As opposed to the resonant case (Fig. 2), there is no measurable difference between the dots and the solid line for the entire length of the plasma. Within the accuracy of the measurement, the instantaneous phase velocity of the wave is constant and is equal to the group velocity of the laser pulse $v_{\mathrm{ph}}=v_g\cong 0.996c$ at $n=7n_{\mathrm{res}}$. This measurement was performed for other phases (crests) of the plasma wave with the same result. The electric field $E_x$ that interacts with an externally injected relativistic electron is shown by the dotted line in Fig. 8 versus the position of the electron in the plasma. As opposed to the resonant case of Fig. 3, the electric field associated with the non-resonant wave does not change polarity at any position $x$ of the injected electron in the plasma. Instead, the profile of the electric field resembles the distribution (profile) of the pump laser pulse. The solid line in Fig. 8 shows a snapshot

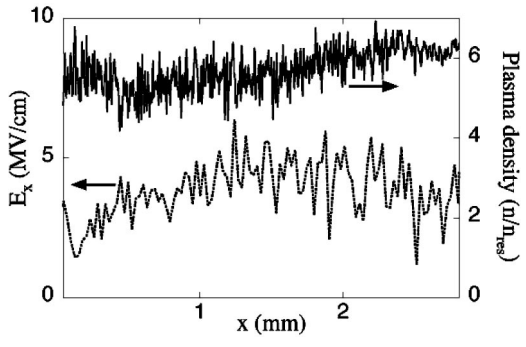


FIG. 8. Longitudinal electric field $E_x$ seen by a "virtual" relativistic electron injected on-axis at $x=0$ and $t\cong 47.5$ ps at the speed of light versus its position $x$ in the plasma (left axis, dotted line) for $n=7n_{\mathrm{res}}$. Axial profile of the plasma density, normalized to $n_{\mathrm{res}}$, at the injection time (right axis, solid line).

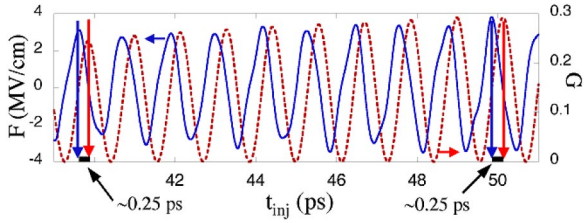


FIG. 9. The solid curve (left axis) shows the trajectory-averaged electric field $F$ seen by a relativistic electron injected on axis (at $x=0$) versus the injection time $F=F(t_{\mathrm{inj}})$. The dotted curve (right axis) shows the trajectory-averaged normalized laser intensity $G$ that the electron is riding along with in the plasma, versus the injection time $G=G(t_{\mathrm{inj}})$. The initial plasma density is $n=7n_{\mathrm{res}}$. The constant separation of $\sim 0.25$ ps between the maxima of $F$ and $G$ (and the phase) is indicated by the vertical arrows.

of the inhomogeneous plasma density on axis at the moment of injection $t\cong 47.5$ ps.

In the case of nonresonant excitation, depending on their moment of injection, the electrons are either constantly accelerated or constantly decelerated, *regardless* of the plasma density. The trajectory-averaged electric field $F(t_{\mathrm{inj}})$ is shown in Fig. 9 together with the trajectory-averaged normalized laser intensity $G(t_{\mathrm{inj}})$ for the $n=7n_{\mathrm{res}}$ case. The two quantities $F$ and $G$ do not go off phase with one another, as it is the case with the resonant RPW's shown in Fig. 4. This is also observed for simulations performed at other nonresonant plasma densities with laser pulses of various durations and intensities. The maximum trajectory-averaged electric field that can be used to accelerate electrons over the entire interaction length ($\sim 3$ mm) is around 3.5 MV/cm. Overall, a nonresonant PBWA would provide less energy gain than a PBWA operating at resonance, but with much better reproducibility of the energy gain of the phase-locked electrons.

## III. EXPERIMENTS

### A. Thomson scattering

As mentioned earlier, many groups around the world have reported the resonant excitation of RPW's [14–18]. However, no one has observed these beat wave-driven modes at extremely nonresonant plasma densities. Recently, Walton *et al.* [19] diagnosed via forward self-scattering of the pump pulse beat-excited RPW's with a frequency $\Delta\omega$ even though the initial plasma density was approximately 12 times the resonant value. However, in their experiments, the RPW was thought to be excited ultimately by the resonant process, as rapid electron expulsion by the laser pulse resulted in the density within the interaction volume to drop to the resonant value. We have performed experiments in order to see if truly nonresonant RPW's could be driven by the beat-wave excitation process. In our experiment, a $CO_2$ laser pulse is used with a peak intensity of about $10^{15}$ W/cm$^2$ (as opposed to $10^{18}$ W/cm$^2$ in Ref. [19]) which is too low to cause electron cavitation. Furthermore, the ponderomotive blowout is too slow to reduce the plasma density from many times $n_{\mathrm{res}}$ to the resonant density during the duration of the laser pulse. The detection and characterization of the RPW's excited on

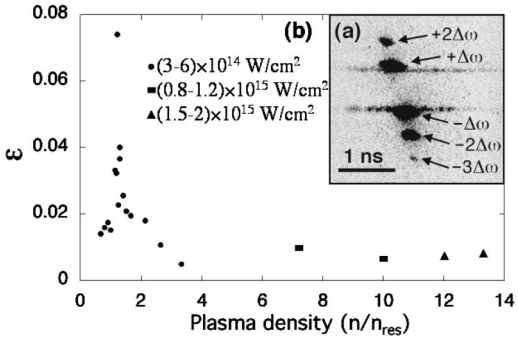


FIG. 10. (a) Time-resolved spectrum of the Thomson scattered light obtained in $He^{1+}$ plasma at a density 5.7 times above resonance. (b) The amplitude of the waves excited in hydrogen versus the plasma density normalized to $n_{\mathrm{res}}$, calculated from the absolute amount of scattered light in the first redshifted sideband for three different intensity ranges of the $CO_2$ laser pulse. The first two sidebands shifted with $\pm\Delta\omega$ are optically attenuated 10 times in (a).

and offresonance was done by probing the plasma wave with photons (Thomson scattering) and by sampling the associated electric fields with injected electrons.

In this experiment, an intense, TW-level $CO_2$ laser pulse operating on 10.3 and 10.6 $\mu$m wavelengths [20] is used to excite the plasma waves. The energy in the two-frequency laser pulse, approximately 100 J, is typically divided in a ratio of 3 (10.6 $\mu$m) to 1 (10.3 $\mu$m). For this pair of lines the resonant density is $9.4\times10^{15}$ cm$^{-3}$. The plasma is produced by tunnel ionization [21] of the fill gas ($H_2$, Ar, or He). The plasma density was directly inferred from the frequency shift acquired by a probe pulse that scatters on the plasma wave excited by the Raman backscattering instability [14]. For these measurements the plasma density was varied from $n_{\mathrm{res}}$ up to $12n_{\mathrm{res}}$. From this diagnostic it could be ascertained that a fully ionized plasma whose density is proportional to the pressure of the fill gas is produced at least at the interaction point of the $CO_2$ and the probe laser pulses [22]. Two different focusing geometries $f/3$ and $f/18$ are used to bring the $CO_2$ beam at a $1/e^2$ intensity spot size of 50 and 200 $\mu$m, respectively. The plasmas are 2–3 mm long for the $f/3$ case and $\sim$40 mm long for the $f/18$ case. The Thomson scattering (TS) measurements are performed with a 532-nm, 20-MW, 2-ns-long probe pulse that propagates collinearly with the $CO_2$ pulse. At the driven frequency, the expected wavelength shift is only 8 Å and therefore a triple-passed Fabry-Perot frequency filter had to be used to separate the intense probe light from the weak scattered light [23]. The detection system is formed by a spectrometer-streak camera combination. The scattering process results in the production of $\sim$100-ps-long sidebands separated with multiples of $\Delta\omega$ as can be seen in Fig. 10(a), which shows a typical $f/3$ time-resolved spectrum of the scattered light at $n=5.7n_{\mathrm{res}}$ in $He^{1+}$ plasma. Similar spectra have been obtained in $H_2$ and Ar. The sidebands are coincident in time; the apparent delay between them is artificially introduced by the TS diagnostic system. No other signals or sidebands (from Raman forward scattering, for example) with amplitudes greater than $5\times10^{-4}$ at $n=10^{17}$ cm$^{-3}$ were detected. The amplitude $\varepsilon$ of the RPW can be estimated for each shot from the power $P_s$ of the scattered light, normalized to the incident power $P_0$ of the probe pulse [24] using the relation

$$\frac{P_s}{P_0}=\left(\frac{\pi}{2}\frac{n}{n_{\mathrm{crit}}}\varepsilon\frac{L}{\lambda_{\mathrm{pr}}}\right)^2, \tag{1}$$

where $n_{\mathrm{crit}}$ is the critical density corresponding to the probe wavelength $\lambda_{\mathrm{pr}}$. Figure 10(b) shows the amplitude of the plasma waves (excited in hydrogen) derived from TS spectra similar to the one shown in Fig. 10(a), as a function of the plasma density (normalized to $n_{\mathrm{res}}$) that covers both the resonant and the nonresonant excitation regimes. For $3n_{\mathrm{res}}<n<14n_{\mathrm{res}}$, the amplitude of the plasma waves was observed to be approximately constant at around 1% ($CO_2$ laser pulses with different intensities were used, see Fig. 10). Since $P_s$ is proportional to $(\varepsilon\times n)^2$, the background plasma density $n$ becomes important for detection purposes. For $n\gg n_{\mathrm{res}}$, even if the amplitude of the RPW is rather small, the recorded $P_s$ is actually significant due to the increased number $\delta n$ of electrons in the wave. The opposite happens for the $n<n_{\mathrm{res}}$ side where $P_s$ decreases rapidly below the detection threshold. The interaction length $L$ used in Eq. (1) was taken to be equal to the Rayleigh range of the $CO_2$ laser beam ($L=1.5$ mm) while the plasma density is taken as that corresponding to the fully ionized neutral density. The plasma wave amplitudes from additional 2D simulations (not shown) performed at parameters close to the experimental shots at nonresonant densities are in reasonable agreement with the amplitudes derived from the TS measurements shown in Fig. 10(b). For densities close to resonance, there appears to be a large disagreement between the experimental data and the results from these simulations that show the existence of RPW's with large amplitudes. It is thought that 3D effects which become increasingly important for large amplitude waves, limited time resolution (100 ps) of the experimental data and shot-to-shot variation in laser parameters (rise time, intensity, and line ratio, not modeled in the simulations), can lead to this discrepancy. However, as stated earlier, nonresonant excitation is not susceptible to these effects to the same extent, which explains a better agreement between the experiment and simulations.

### B. Electron acceleration

As opposed to the TS measurements where the photons in the probe pulse interact with the density perturbation $\delta n$, the electrons that are injected in the plasma interact with the electric fields (both transverse and longitudinal) associated with the RPW. As previously mentioned in Sec. II B, the magnitude of these fields can be found only from the simulation results. In the case of nonresonant excitation for the $f/3$ focusing geometry, the simulations show the existence of longitudinal electric fields $E_x$ of $\sim$2 MV/cm. These fields were probed experimentally by injecting a 12-MeV electron beam produced by a photoinjector that is described elsewhere [25]. Given the small interaction length of $\sim$1.5 mm and the small focal spot leading to strong transverse fields, experimental observation of acceleration of injected elec-

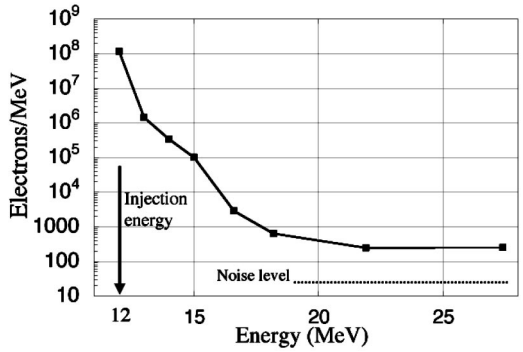


FIG. 11. The spectrum of the accelerated electrons for a two-frequency shot with plasma in $H_2$ at $n=3.3n_{\mathrm{res}}$. The $CO_2$ laser pulse was focused with $f/18$ optics.

trons using this setup proved to be difficult, as the electron beam was strongly defocused. Therefore, the experiment was repeated with the $f/18$ geometry at $n=3.3n_{\mathrm{res}}$ at maximum laser intensities of $8\times10^{14}$ W/cm$^2$.

The 12-MeV electron beam was injected in the plasma produced by the $f/18$ optic collinearly with the $CO_2$ beam with 0.1° alignment accuracy. The 10-ps-long (FWHM) electron bunch, containing up to $3\times10^8$ electrons per shot, was focussed down to a transverse spot size $\sigma_{\mathrm{rms}}=150$ $\mu$m. A correlation technique based on the modulation of transmission of the $CO_2$ laser pulse by the electron pulse in a thin Ge slab [26] was used to synchronize the electrons with the 10-$\mu$m photons with 20 ps uncertainty. Because the duration of the electron pulse is approximately 10 ps, it overlaps with $\geqslant10$ wavelengths of the RPW. The spectrum of the electrons exiting the plasma within a full cone angle of 1° was analyzed using a 0.4 T magnetic field applied by a dipole magnet with Browne and Buschner pole pieces (with imaging properties in the energy plane) in combination with a set of Si surface barrier detectors (SBD's) and two fluorescent screens with different sensitivities. One screen was used to detect electrons with energies of $\sim12$ MeV (injection energy), and the other, approximately 100 times more sensitive, detected electrons with energies from 12.5 to 15 MeV. The number of electrons/mm$^2$ striking either fluorescer was estimated by converting the brightness of the fluorescence produced by the electrons using experimentally determined fluorescence efficiency. The SBD's, calibrated with a $\beta$ source, were used to detect electrons with energies higher than 15 MeV. Special care was taken in shielding the SBD's against stray 12-MeV electrons and x rays that were produced during the shots. No significant signals above the noise level were measured on the detectors when there was no plasma but a beat wave and an electron beam; or plasma produced by a single frequency pulse and an electron beam; or plasma produced by a beat wave but no injected electron beam.

The number of electrons was estimated on the fluorescent screens at four predefined positions 12, 13, 14, and 15 MeV. Together with the signals from the calibrated SBD detectors, the spectrum of the accelerated electrons, shown in Fig. 11, was constructed for a beat-wave shot taken in hydrogen at $n=3.3n_{\mathrm{res}}$. Electrons with a maximum energy of up to 28 MeV, i.e., an overall energy gain of 16 MeV (approximately 2.5 times less than the gain obtained at resonance [27]), were seen. Therefore, the nonresonantly excited RPW's produced an average $E_x$ of 4 to 8 MV/cm if an interaction length of 4 to 2 cm is assumed. From additional $f/18$ TS measurements, the amplitude of the plasma wave was estimated to be 1–2 %. The corresponding electric field would then be up to 6.6 MV/cm in the 1D approximation which is valid for the large spot sizes produced by the $f/18$ optics. This value of the electric field is in reasonable agreement with the data from the electron spectrum as well as the results ($E_x$) from the 2D simulations of this case (not shown).

## IV. CONCLUSIONS

In conclusion, we have studied the nonresonant excitation of RPW's using both simulations and experiments. The results from the 2D simulations performed at plasma densities much higher than the resonant density show that RPW's having the same frequency and wave number as the beat pattern of the pump laser pulse are excited. The phase velocity of these waves is equal to the group velocity of the laser pulse in the plasma and is, therefore, constant and nearly independent of the spatial and temporal variations of the plasma density. These plasmons are always phase locked with respect to the driving electromagnetic beat wave, which in turn makes them well suited for the acceleration of phased-locked electrons. Although the amplitude $\delta n/n$ of these waves is small, the longitudinal electric fields associated with them can be quite significant (100 s of MV/m), depending on the intensity of the laser pulse. Experimentally, such waves have been excited using a two-frequency $CO_2$ laser pulse over a wide range of densities up to 14 times above the resonant density of $9.4\times10^{15}$ cm$^{-3}$. These RPW's have been diagnosed using collinear Thomson scattering and their electric fields probed by injecting relativistic electrons. From the energies gained by the injected electrons, accelerating gradients of 400–500 MeV/m are inferred.

The amplitude of these RPW's could be significantly increased using more powerful laser pulses. 2D simulations using 25 ps laser pulses with $a_1=a_2=0.6$ show that nonresonant fields up to 4.5 GV/m could be reached at a plasma density $n=10n_{\mathrm{res}}$. The excitation of such high-amplitude electric fields in these simulations was aided by the onset of relativistic self-focusing at these higher densities. According to Ref. [28], the self-focussing threshold for a $10^{17}$ cm$^{-3}$ plasma is only 1.7 TW, a power level achievable today for $CO_2$ lasers. It should be noted that the wavelength of the nonresonant mode remains equal to the spacing between the beats in the drive pulse and, for $n=10n_{\mathrm{res}}$, is $10^{1/2}$ times longer than the wavelength of the RPW that could be resonantly excited at that higher density. As a result of this longer wavelength (at the expense of smaller fields), it may be easier to inject pre-bunched electrons into such a nonresonant wave. The amount of laser power delivered to the interaction volume for the excitation of the RPW could be limited by the ionization induced refraction phenomenon [29] if the plasma is to be created by the laser pulse itself by tunneling ionization. However, regardless of the technique used to propagate an intense laser pulse through a rather high-

density plasma, the RPW's excited off resonance are nearly insensitive to variations in the plasma density. This makes the acceleration of phase-locked electrons using nonresonant RPW's very attractive for plasma channels. Such nonresonantly excited RPW's could be desirable for second generation PBWA experiments whose goal is to demonstrate nearly monoenergetic, high-gradient acceleration of phase-locked electrons.

**ACKNOWLEDGMENTS**

The authors would like to thank Dr. D. Gordon for help with the simulations and Professors W. Mori and T. Katsouleas for useful discussions. This research was supported by the U.S. Department of Energy under Contract No. DE-FG03-92ER40727.

[1] T. Tajima and J. M. Dawson, Phys. Rev. Lett. **43**, 267 (1979).
[2] E. Esarey *et al.*, IEEE Trans. Plasma Sci. **24**, 252 (1996).
[3] C. Joshi *et al.*, Nature (London) **311**, 525 (1984).
[4] C. E. Clayton *et al.*, Phys. Rev. Lett. **70**, 37 (1993).
[5] F. Amiranoff *et al.*, Phys. Rev. Lett. **74**, 5220 (1995).
[6] S. Ya. Tochitky *et al.*, *Advanced Accelerator Concepts*, AIP Conf. Proc. No. 647, edited by C. E. Clayton and P. Muggli (AIP, Melville, 2002), pp. 786–795.
[7] D. Gordon *et al.*, Phys. Rev. E **57**, 1035 (1998).
[8] M. N. Rosenbluth and C. S. Liu, Phys. Rev. Lett. **29**, 701 (1972).
[9] C. M. Tang *et al.*, Phys. Fluids **28**, 1974 (1985).
[10] S. J. Karttunen and R. R. E. Salomaa, Phys. Scr. **39**, 741 (1988).
[11] C. Joshi *et al.*, Comments Plasma Phys. Controlled Fusion **16**, 65 (1994).
[12] C. E. Clayton *et al.*, Phys. Plasmas **1**, 1753 (1994).
[13] D. F. Gordon *et al.*, IEEE Trans. Plasma Sci. **28**, 1135 (2000).
[14] C. E. Clayton *et al.*, Phys. Rev. Lett. **54**, 2343 (1985).
[15] A. E. Dangor *et al.*, Phys. Scr. **T30**, 107 (1990).
[16] F. Moulin *et al.*, Phys. Plasmas **1**, 1318 (1994).
[17] Y. Kitagawa *et al.*, Phys. Rev. Lett. **68**, 48 (1992).
[18] N. A. Ebrahim, J. Appl. Phys. **76**, 7645 (1994).
[19] B. Walton *et al.*, Opt. Lett. **27**, 2203 (2002).
[20] S. Ya. Tochitsky *et al.*, Opt. Lett. **26**, 813 (2001).
[21] W. P. Leemans *et al.*, Phys. Rev. Lett. **68**, 321 (1992).
[22] C. V. Filip *et al.*, in *Advanced Accelerator Concepts* [6] pp. 770–785.
[23] C. V. Filip *et al.*, Rev. Sci. Instrum. **74**, 3576 (2003).
[24] R. E. Slusher and C. M. Surko, Phys. Fluids **23**, 472 (1980).
[25] S. G. Anderson *et al.*, in *Advanced Accelerator Concepts*, AIP Conf. Proc. No. 569, edited by P. L. Colestock and S. Kelly (AIP, Melville, 2000), pp. 487–499.
[26] P. B. Corkum *et al.*, J. Appl. Phys. **50**, 3079 (1979).
[27] S. Ya. Tochitsky *et al.*, Phys. Rev. Lett. (to be published).
[28] P. Sprangle *et al.*, Phys. Rev. Lett. **69**, 2200 (1992).
[29] W. P. Leemans *et al.*, Phys. Rev. A **46**, 1091 (1992).